On the motion of slender vortex filaments

Hong Zhou
Department of Mathematics, University of California and Lawrence Berkeley National Laboratory, Berkeley, California 94720

(Received 7 March 1996; accepted 6 November 1996)

Several approaches for slender vortex motion (the local induction equation, the Klein–Majda equation, and the Klein–Knio equation) are compared on a specific example of sideband instability of Kelvin waves on a vortex. Numerical experiments on this model problem indicate that all these equations yield qualitatively similar behavior, and this behavior is different from the behavior of a nonslender vortex with variable cross-section. It is found that the boundaries between stable, recurrent, and chaotic regimes in the parameter space of the model problem depend on the equation used. The boundaries of these domains in the parameter space for the Klein–Majda equation and for the Klein–Knio equation are closely related to the core size. When the core size is large enough, the Klein–Majda equation always exhibits stable solutions for our model problem. Various conclusions are drawn; in particular, the behavior of turbulent vortices cannot be captured by these approximations, and probably cannot be captured by any slender vortex model with constant vortex cross-section. Speculations about the differences between classical and superfluid hydrodynamics are also offered. [S1070-6631(97)00803-9]

I. INTRODUCTION

Fluid vorticity is often concentrated in small regions. The special case where vorticity is concentrated on a single slender filament is important in many problems (e.g. turbulence, superfluidity). The study of the motion of slender vortices has received a lot of attention. The local induction equation,[1] the Klein–Majda equation,[2] and the Klein–Knio equation[3] are three different approximations for the motion of slender vortices. The comparison of these models and the study of differences between the results by these models and what we expect in turbulence theory are the main goals of this paper.

The paper is organized as follows. After a brief review of vortex dynamics, we present approximate equations of motion for slender vortices, namely, the self-induction equation, the Klein–Majda equation and the Klein–Knio equation. The third section describes a model problem which comes from the theory of vortex wave motion in superfluid helium. The equations are applied to the model problem, and the results are displayed. We then draw various conclusions from these results.

We consider unbounded, inviscid, incompressible flows. In the absence of external force, the motion of such fluid with unit density is described by the Euler equations:

$$\frac{D\mathbf{u}}{Dt} = -\nabla\, p, \tag{1}$$

$$\nabla\cdot\mathbf{u} = 0, \tag{2}$$

where $\mathbf{u}(\mathbf{x},t)$ is the velocity, $\mathbf{x}=(x_1,x_2,x_3)$ is the position, p is the pressure, $\nabla=(\partial/\partial x_1,\partial/\partial x_2,\partial/\partial x_3)$ is the differentiation vector, t is the time, and $D/Dt\equiv\partial_t+\mathbf{u}\cdot\nabla$ is the material derivative.

The curl of the velocity field,

$$\boldsymbol{\omega}=\nabla\times\mathbf{u} \tag{3}$$

is the vorticity. The velocity $\mathbf{u}(\mathbf{x})$ can be determined from the vorticity $\boldsymbol{\omega}(\mathbf{x})$ through the Biot–Savart law:

$$\mathbf{u}(\mathbf{x}) = -\frac{1}{4\pi}\int \frac{(\mathbf{x}-\mathbf{x}')\times\boldsymbol{\omega}(\mathbf{x}')}{|\mathbf{x}-\mathbf{x}'|^3}\, d\mathbf{x}'. \tag{4}$$

If the vorticity is concentrated on a single thin filament C of circulation Γ, Eq. (4) becomes

$$\mathbf{u}(\mathbf{x}) = -\frac{\Gamma}{4\pi}\int_C \frac{(\mathbf{x}-\mathbf{x}')\times d\mathbf{l}(\mathbf{x}')}{|\mathbf{x}-\mathbf{x}'|^3}. \tag{5}$$

If self-induced motion of the line filament is calculated by evaluating the velocity from (5) on the filament itself, the result will be logarithmically infinite if the filament is curved and zero if it is straight. Thus, self-induced motion occurs only for curved filaments. But to obtain the correct value for the velocity, further considerations of the finite size of the vortex core as well as the vorticity distribution are required.

In this paper we focus our attention on very thin vortex filaments. We shall use the term *thin* or *slender* to describe any vortex filament with a typical radius of the core that is small compared to a characteristic radius of curvature. Thin vortices are very important in many respects. It has been suggested by Chorin and Akao[4] that thin vortices play an important role in the structure of turbulent flows.

Vortex motion in three-dimensional space differs from vortex motion in two dimensions in several ways; the most significant result from vortex stretching.[5] Vortex stretching causes vortex folding and the temperature is decreased.[6,7] As time $t\to\infty$, a statistically steady state can be expected for a vortex filament system.[8,9] By contrast, superfluid vortices are nearly true lines, and with some exceptions (i.e., near the critical temperature) they generally look smoother than classical vortices and remain relatively ordered. Unlike in fluid mechanics where a classical fluid has a self-adjusting temperature, a superfluid has a fixed temperature and the constant temperature of superfluid vortex states should inhibit vortex stretching. The cause of the differences in dynamical

 1070-6631/97/9(4)/970/12/$10.00

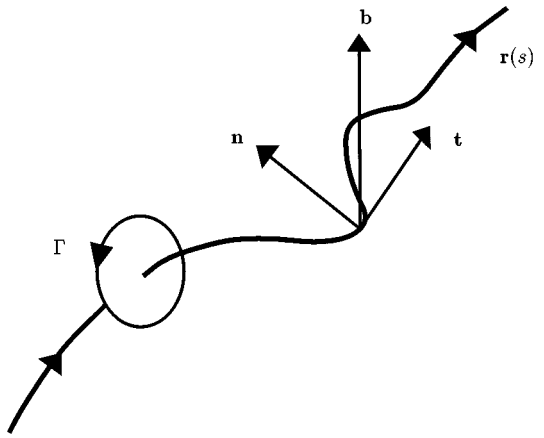

FIG. 1. Definitions for the local induction approximation (LIA).

behavior between superfluid vortices and classical vortices remains a mystery. In this paper we try to give some suggestions.

II. EQUATIONS OF MOTION FOR THIN VORTICES

The simulation of the motion of a very slender vortex filament by using the classic vortex method would be prohibitively expensive due to the overlapping condition of the vortex method.[10] For our model problem which will be discussed in Sec. V, the number of vortex elements required by the vortex method in a fairly coarse spatial discretization is over 10^6. Even with the help of a fast vortex method,[11] a simulation with such a large number of numerical vortex elements is still not realistic. Therefore, approximate equations are developed to replace the Biot–Savart law. Three modeling approaches are adopted in this section to analyze the motion of slender vortex filaments. The first is the local induction approximation (LIA), which leads to a cubic nonlinear Schrödinger equation. The second is due to Klein and Majda, who derived a more accurate asymptotic equation for the motion of thin vortex filaments. The third approach, credited to Klein and Knio, takes the core vorticity structure into consideration. It should be pointed out that all of these three equations assume that the core size is small compared with the radius of curvature. According to the stability analysis given by Widnall *et al.*[12] and Wang,[13] instability occurs when the wavelength is comparable with the core size of the vortex filament. Hence, it is plausible to conjecture that hairpins might not develop when the core size is very small, even though Klein and Majda[16] claimed that hairpins appear in their model.

To start with, consider a vortex filament described by $\mathbf{r}(s)$, where s is an arc length parameter measured along the filament and $\mathbf{r}(s)$ is the position vector. Let $\mathbf{t}$, $\mathbf{n}$, $\mathbf{b}$ denote the unit tangent, normal, and binormal vectors, respectively (see Fig. 1).

One way to avoid singularity in Eq. (5) is to simply ignore the nonlocal contribution of the filament and replace the Biot–Savart law (5) by a velocity expression that depends only on the local curvature of the vortex filament. This leads to the local induction approximation, which reads[1]

$$\frac{\partial \mathbf{r}}{\partial t} = \kappa \mathbf{b} = \mathbf{t} \times \frac{\partial \mathbf{t}}{\partial s}, \tag{6}$$

where κ is the curvature. Equation (6) has a very different character from the Euler equations, and in particular it preserves vortex length.[14]

Differentiation of both sides of (6) with respect to arc length s gives the local induction equation in terms of the tangent vector:

$$\frac{\partial \mathbf{t}}{\partial t} = \mathbf{t} \times \frac{\partial^2 \mathbf{t}}{\partial s^2}. \tag{7}$$

Hasimoto[15] has shown elegantly that Eq. (6) can be reduced to a cubic nonlinear Schrödinger equation (NLSE)

$$\frac{1}{i}\frac{\partial \phi}{\partial t} = \frac{\partial^2 \phi}{\partial s^2} + \frac{1}{2}\phi |\phi|^2 \tag{8}$$

where ϕ is the complex function defined in terms of the filament curvature κ and torsion τ:

$$\phi = \kappa \exp\left(i \int_0^s \tau ds \right). \tag{9}$$

We call (9) the *Hasimoto transformation* and ϕ the *filament function* which contains all the geometrical information for the filament.

While the local induction approximation does not allow for any vortex stretching, numerical simulations indicate that vortex stretching occurs for moderately thin vortex filaments in incompressible fluids.[7] To retain vortex stretching, Klein and Majda[2] developed an asymptotic theory for slender vortex filaments.

The slender vortices in the Klein–Majda regime are, to leading order, straight vortex filaments that are subject to small amplitude displacements. The displacement of the vortex filament centerlines away from the straight reference lines may be, but is not necessarily, large in comparison with

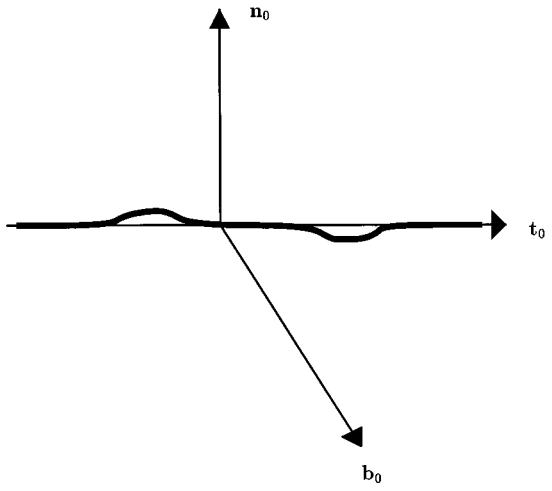

FIG. 2. A special perturbation of the straight reference filament: $(\mathbf{t}_0, \mathbf{n}_0, \mathbf{b}_0)$ form a right-handed orthonormal basis, $\mathbf{x}^{(2)}(\sigma,\tau) = \alpha(\sigma,\tau)\mathbf{n}_0 + \beta(\sigma,\tau)\mathbf{b}_0$.

a typical core size of the filament but it must be small compared to a typical perturbation wavelength. In turn, the perturbation wavelengths are small compared to a characteristic radius of curvature of the filament. Thus with lengths measured on the curvature scale, the slender vortices in the Klein–Majda regime are characterized by *small amplitude–short wavelength* distortions of a slender columnar vortex.

Following Klein and Majda,[2] we assume the centerline of a slender vortex filament, $L^{\varepsilon}(t): s \to \mathbf{x}(s,t;\varepsilon)$, is described by (Fig. 2)

$$\mathbf{x}(s,t;\varepsilon) = \varepsilon\sigma\mathbf{t}_0 + \varepsilon^2\mathbf{x}^{(2)}(\sigma,\tau) + o(\varepsilon^2), \tag{10}$$

where $\mathbf{x}$ is the position vector, $\sigma = s/\varepsilon$ and $\tau = t/\varepsilon^4$ are the scaled space and time coordinates, $\mathbf{t}_0$ is a constant unit vector, and ε is a perturbation scaling parameter which satisfies $\varepsilon \ll 1$. The vortex core size δ and the parameter ε are linked through the distinguished limit[2]

$$\varepsilon^2 = \frac{1}{\ln\dfrac{2\varepsilon}{\delta} + C}, \tag{11}$$

where C is a constant.

When the potential flow at infinity is zero, the filament motion obeys the perturbed binormal law

$$\frac{\partial \mathbf{x}(s,t)}{\partial t} = \kappa\mathbf{b}(s,t) + \varepsilon^2\mathbf{v}(s,t), \tag{12}$$

where $\varepsilon^2\mathbf{v}(s,t)$ is a small perturbation velocity. Using the curve representation (10) and by the method of asymptotic expansions, one finds

$$\mathbf{v} = I[\mathbf{x}^{(2)}] \times \mathbf{t}_0. \tag{13}$$

Here the linear nonlocal operator $I[\,\cdot\,]$ is defined by

$$I[w](\sigma) = \int_{-\infty}^{\infty} \frac{1}{|h^3|}\Big[w(\sigma+h) - w(\sigma) - hw'(\sigma+h) + \frac{h^2}{2}H(1-|h|)w''(\sigma)\Big]dh, \tag{14}$$

where the notation $' = \partial/\partial\sigma$ and H is the Heaviside function. Therefore, the nonlocal contribution of the filament is replaced by I, whose effect can be understood by considering its Fourier symbol:

$$\hat{I}(\xi) = \int_{\mathbf{R}} e^{-i\sigma\xi} I(\sigma)\,d\sigma = |\xi|^2(-\ln|\xi| + C_0), \tag{15}$$

where $C_0 = 1/2 - \gamma$, and γ is Euler's constant.

Klein and Majda showed that Hasimoto's transformation (9) turns the evolution Eq. (12) with $\mathbf{v}$ from (13) into the perturbed nonlinear-nonlocal Schrödinger equation

$$\frac{1}{i}\frac{\partial\phi}{\partial\tau} = \frac{\partial^2\phi}{\partial\sigma^2} + \varepsilon^2\left(\tfrac{1}{2}\phi|\phi|^2 - I[\phi]\right). \tag{16}$$

We call (16) the *Klein–Majda equation*. In this equation, the nonlocal term $I[\phi]$ directly competes with the cubic nonlinearity. Thus, the nonlocal contributions become as important as the nonlinear local induction effects. Furthermore, it is shown that the nonlocal term $-\varepsilon^2 I[\phi]$ is responsible for the local self-stretching of filament. It is also shown by Klein and Majda[2] that the nonlocal operator generates a highly singular perturbation of the NLSE (8). According to the numerical calculations presented in Klein and Majda,[16] the filament function ϕ develops higher and much narrower peaks as time evolves when compared with the corresponding solutions of NLSE; and these curvature peaks may correspond to the birth of small scale ''hairpins'' or kinks along the actual vortex filament.

Recently Klein and Knio[3] proposed a model for slender vortex motion. Their model gives an asymptotically correct account of the local effect and an exact account of the nonlocal effect. More importantly, it represents the influence of the vortex core structure on the vortex filament motion, including a nontrivial axial flow. By combining a thin-tube method[17] with their asymptotic analysis, Klein and Knio also presented several numerical methods for solving their model equation. Most recently, Klein, Knio, and Ting[18] proposed a model that allows an accurate description of the effects of axial flow in core, viscosity and vortex stretching on slender vortex filament motion. Here we consider the inviscid evolution of slender vortex filament with no axial flow.

Detailed asymptotic analyses[3] show that under certain conditions of quasi-steadiness, the velocity of a slender vortex filament is

$$\mathbf{u}(\mathbf{x}) = \frac{\Gamma}{4\pi}\left[\ln\left(\frac{2}{\delta}\right) + C\right]\kappa\mathbf{b} + Q^f(\mathbf{x}). \tag{17}$$

Here Γ is the circulation of the vortex, κ and $\mathbf{b}$ denote respectively the local curvature and the unit binormal vector at $\mathbf{x}$. The quantity C is a core structure coefficient given by

$$C = \lim_{r\to\infty}\left(\frac{4\pi^2}{\Gamma^2}\int_0^r r' v^{(0)2} dr' - \ln r\right) - \frac{1}{2} - \frac{8\pi^2}{\Gamma^2}\int_0^{\infty} r' w^{(0)2} dr', \tag{18}$$

where $v^{(0)}$, $w^{(0)}$ are the leading order axisymmetric axial and circumferential velocities in the vortex core, $r' = r/\delta$, and δ is the core radius. The last term $Q^f(\mathbf{x})$ in (17) is the finite part of the line Biot–Savart integral, which reflects the nonlocal contribution to the self-induced velocity. For convenience, we shall call Eq. (17) the *Klein–Knio equation*, even though it first appeared in Callegari and Ting.[19]

To solve Eq. (17) for slender vortex motion, Klein and Knio developed a method based on the thin-tube method. Before introducing Klein and Knio's method, we briefly review the thin-tube method.

The standard thin-tube method[17] is a simplified version of general vortex element method[20] for three-dimensional incompressible flows. In the thin-tube model, a slender vortex is represented by a single chain of overlapping vortex elements. Each element is a circular cylinder characterized by a circulation Γ equal to the flux of vorticity across its cross section and by two Lagrangian variables which describe the endpoints of the associated line segment. The Lagrangian variables are moving with the fluid and can be denoted by

χ_i, $i=1,2,\ldots,N$. The vortex elements are ordered so that the indices increase in the direction of the vorticity. Therefore, the vorticity can be discretized as

$$\boldsymbol{\omega}(\mathbf{x},t)=\sum_{i=1}^{N}\Gamma\,\delta\chi_i(t)f_\delta(\mathbf{x}-\chi_i^c(t)). \tag{19}$$

In this expression, f_δ is a smooth approximation to the Dirac delta function with a cutoff radius δ and is formed as

$$f_\delta(\mathbf{x})=\frac{1}{\delta^3}f\left(\frac{|\mathbf{x}|}{\delta}\right), \tag{20}$$

and

$$\delta\chi_i(t)=\chi_{i+1}(t)-\chi_i(t), \tag{21}$$

$$\chi_i^c(t)=\frac{\chi_{i+1}(t)+\chi_i(t)}{2}, \tag{22}$$

denote respectively the length and center of the ith vortex element. The smoothing function $f(\mathbf{x})$ is chosen so as to enhance accuracy.[20] The velocity at a point $\mathbf{x}$ can be obtained by inserting (19) into (5) and performing the integration. The result is the following desingularized version of the Biot–Savart law:

$$\mathbf{u}(\mathbf{x},t)=-\frac{1}{4\pi}\sum_{i=1}^{N}\Gamma\,\frac{(\mathbf{x}-\chi_i^c(t))\times\delta\chi_i^c(t)}{|\mathbf{x}-\chi_i^c(t)|^3}\times K_\delta(\mathbf{x}-\chi_i^c(t)), \tag{23}$$

where

$$K_\delta(\mathbf{x})\equiv K\left(\frac{|\mathbf{x}|}{\delta}\right) \tag{24}$$

and $K(r)$ is the velocity smoothing kernel corresponding to the vorticity smoothing kernel:

$$K(r)=4\pi\int_0^r\overline{r^2}f(\overline{r})d\overline{r}. \tag{25}$$

The calculated velocity $\mathbf{u}(\chi_i)$ is used to advance χ_i.

In the above standard thin-tube method, the cutoff radius is usually chosen to be the physical vortex core radius. Klein and Knio found that this choice, in general, leads to an $O(1)$ error due to the differences between the physical and numerical core structures.[3] So the velocity given by the thin-tube method has to be corrected.

Let $\mathbf{u}^{\mathrm{ttm}}$ denote the velocity obtained from the thin-tube method (23), and let C, C^{ttm} denote respectively the physical and numerical core structure coefficients. The modifications of the thin-tube model derived by Klein and Knio can be summarized into the following form:

$$\mathbf{u}=\mathbf{u}^{\mathrm{ttm}}+\frac{\Gamma}{4\pi}\left(C-C^{\mathrm{ttm}}+\ln\frac{\delta^{\mathrm{ttm}}}{\delta}\right)\kappa\mathbf{b}, \tag{26}$$

where $\mathbf{u}$ at the left-hand side is the true (corrected) velocity of the filament.

If δ^{ttm} is chosen to be δ, then

$$\mathbf{u}=\mathbf{u}^{\mathrm{ttm}}+\frac{\Gamma}{4\pi}(C-C^{\mathrm{ttm}})\kappa\mathbf{b}. \tag{27}$$

Therefore, when we use the standard thin-tube method with $\delta^{\mathrm{ttm}}=\delta$, we have to add an explicit correction velocity to the numerical velocity $\mathbf{u}^{\mathrm{ttm}}$.

If δ^{ttm} is chosen so that $C-C^{\mathrm{ttm}}+\ln(\delta^{\mathrm{ttm}}/\delta)=0$, then $\mathbf{u}=\mathbf{u}^{\mathrm{ttm}}$. In other words, if we use a rescaled numerical core radius

$$\delta^{\mathrm{ttm}}=\delta\exp(C-C^{\mathrm{ttm}}), \tag{28}$$

the standard thin-tube method can be applied directly without correction. This method is attractive since it does not contain a correction term which involves numerical calculations of curvature and binormal vector.

In Eq. (26), the choice of the numerical core radius δ^{ttm} is not fixed. This could be very helpful when the physical core radius δ is extremely small (e.g., superfluid vortices). In the two particular methods of correction described by (27) and (28), the numerical core radius δ^{ttm} is either exactly equal to or of the same order as the physical core radius δ. When δ is very small, the overlapping condition required by the thin-tube method makes numerical simulations virtually impossible. In the numerical experiments presented in this paper, the ratio of the physical core radius to the period of the solution is of the order 10^{-5}. Obviously, one cannot afford to use δ^{ttm} that small. We shall use a moderately small δ^{ttm} in the thin-tube method and then do correction according to (26).

III. NUMERICAL SOLUTIONS OF THE APPROXIMATE EQUATIONS

The method we use to solve the local induction approximation is due to Buttke.[14] Instead of solving for the position vector $\mathbf{r}$, Buttke's method solves for the tangent vector $\mathbf{t}$ as in Eq. (7).

Let $\mathbf{t}_j^n$ denote the approximation to $\mathbf{t}(j\Delta s,n\Delta t)$. Buttke developed a Crank–Nicholson type scheme:

$$\mathbf{t}_j^{n+1}-\mathbf{t}_j^n=\frac{\Delta t}{4(\Delta s)^2}(\mathbf{t}_j^{n+1}+\mathbf{t}_j^n)\times(\mathbf{t}_{j+1}^{n+1}+\mathbf{t}_{j-1}^{n+1}+\mathbf{t}_{j+1}^n+\mathbf{t}_{j-1}^n), \tag{29}$$

where Δs is the spatial increment and Δt is the temporal increment.

In Eq. (29), $\{\mathbf{t}_j^{n+1}\}$ can be solved by two iterative methods. Both methods produce a sequence of unit vectors $\mathbf{x}_j^k$ which converges to $\mathbf{t}_j^n$, provided Δt is appropriately restricted.

Let $\mathbf{x}_j^0=\mathbf{t}_j^n$. In the first iterative method, given unit vector $\mathbf{x}_j^n$, we define $\mathbf{x}_j^{k+1}$ by the equation

$$\mathbf{y}_j^{k+1}-\mathbf{t}_j^n=\frac{\Delta t}{4(\Delta s)^2}(\mathbf{x}_j^k+\mathbf{t}_j^n)\times(\mathbf{x}_{j+1}^k+\mathbf{x}_{j-1}^k+\mathbf{t}_{j+1}^n+\mathbf{t}_{j-1}^n) \tag{30}$$

and

$$\mathbf{x}_j^{k+1}\equiv\frac{\mathbf{y}_j^{k+1}}{|\mathbf{y}_j^{k+1}|}. \tag{31}$$

It can be shown[21] that $\mathbf{x}_j^n\to\mathbf{t}_j^{n+1}$ if $\Delta t<(\Delta s)^2/4$.

In the second iterative method, we define the sequence of unit vectors $\mathbf{x}_j^k$ by

$$\mathbf{x}_j^{k+1}-\mathbf{t}_j^n=\frac{\Delta t}{4(\Delta s)^2}(\mathbf{x}_j^{k+1}+\mathbf{t}_j^n)$$
$$\times(\mathbf{x}_{j+1}^k+\mathbf{x}_{j-1}^k+\mathbf{t}_{j+1}^n+\mathbf{t}_{j-1}^n). \tag{32}$$

The sequence $\mathbf{x}_j^k$ obtained in this manner[21] converges to $\mathbf{t}_j^{n+1}$ if $\Delta t<(\Delta s)^2$.

For the Klein and Majda equation (16), we use a fractional step method developed by Klein and Majda.[16] The method is designed for general periodic initial data. It consists of two steps. In the first fractional step, we solve the Fourier transform of the linear problem

$$\frac{1}{i}\frac{\partial\phi}{\partial\tau}=\frac{\partial^2\phi}{\partial\sigma^2}-\varepsilon^2 I[\phi] \tag{33}$$

exactly for the discrete Fourier modes $\{\hat{\phi}_l\}$ of data $\{\phi_l\}$ on an equi-distance grid. The Fourier modes $\{\hat{\phi}_l\}$ are obtained by applying the discrete fast Fourier transform (DFFT) to $\{\phi_l\}$. The exact solution for $\hat{\phi}_l$ is given by

$$\hat{\phi}_l(\tau+\Delta\tau)=\hat{\phi}_l(\tau)\exp(-i[l^2+\varepsilon^2\hat{I}(l)]\Delta\tau). \tag{34}$$

After $\{\hat{\phi}_l\}$ has been advanced from τ to $\tau+\Delta\tau$, an inverse Fourier transform (IFFT) is employed to calculate $\{\phi_l(\tau+\Delta\tau)\}$ from $\{\hat{\phi}_l(\tau+\Delta\tau)\}$.

In the second fractional step, we solve the nonlinear ODE

$$\frac{1}{i}\frac{\partial\phi}{\partial\tau}=\varepsilon^2\frac{1}{2}\phi|\phi|^2 \tag{35}$$

exactly at each discrete spatial location by

$$\phi_l(\tau+\Delta\tau)=\phi_l(\tau)\exp(i\varepsilon^2\tfrac{1}{2}|\phi_j(\tau)|^2\Delta\tau). \tag{36}$$

The two steps are alternated in time through a Strang-type splitting. The method is second order accurate and unconditionally stable. An adaptive time step $\Delta\tau$ is chosen by

$$\Delta\tau=s\frac{2\pi}{w^*}\frac{1}{N}. \tag{37}$$

In Eq. (37), s is a safety factor (say $s=0.5$), N is the number of grid points and w^* is the weighted average frequency

$$w^*=\max\left(-\int\hat{w}(\xi)|\hat{\phi}|^2(\xi)d\xi/\|\phi\|_{L^2}^2,\right.$$
$$\left.\int w(|\phi|)|\hat{\phi}|^2 d\sigma/\|\phi\|_{L^2}^2\right), \tag{38}$$

where $\hat{w}$, w are the frequencies in the fractional step solution formulas (34) and (36).

Once the filament function ϕ is known, one can determine the filament position using the Serret–Frenet equations.[23]

To solve the Klein–Knio equation (17), we use a thin-tube method with a moderately small numerical core radius δ^{ttm} and then make correction according to (26). The correction term in (26) is roughly

$$\frac{\Gamma}{4\pi}\ln\frac{\delta^{\text{ttm}}}{\delta}\boldsymbol{\kappa}\mathbf{b}. \tag{39}$$

For the LIA equation $\mathbf{u}=\boldsymbol{\kappa}\mathbf{b}$, the time step Δt is restricted by $\Delta t<O((\Delta s)^2)$.[14] Thus for the velocity given by (39), in order to maintain the numerical stability, the time step Δt has to be restricted by

$$\Delta t<\frac{1}{\dfrac{\Gamma}{4\pi}\ln\dfrac{\delta^{\text{ttm}}}{\delta}}O((\Delta s)^2). \tag{40}$$

When δ is extremely small, the coefficient in front of $\boldsymbol{\kappa}\mathbf{b}$ in (39) is large. That means, for the velocity given by (39), the time step Δt has to be a tiny fraction of $(\Delta s)^2$. In the numerical experiment using the thin-tube method without correction term, we found that we can take fairly large time step Δt without suffering from the numerical instability. It makes sense to use a larger time step for $\mathbf{u}^{\text{ttm}}$ in (26) and use a smaller time step for the correction term in (26). Note that the direct evaluation of $\mathbf{u}^{\text{ttm}}$ in (26) costs $O(N^2)$ operations, while it takes only $O(N)$ operations to compute the correction term. Thus we use a hybrid of a fractional step method and a high order Runge–Kutta method to solve (26). In the first fractional step, we solve

$$\frac{d\mathbf{x}}{dt}=\mathbf{u}^{\text{ttm}} \tag{41}$$

by an embedded Runge–Kutta method[22] for one step with step size Δt. In the second fractional step, we solve

$$\frac{d\mathbf{x}}{dt}=\frac{\Gamma}{4\pi}(\boldsymbol{\kappa}\mathbf{b})\left[C-C^{\text{ttm}}+\ln\frac{\delta^{\text{ttm}}}{\delta}\right] \tag{42}$$

by the same embedded Runge–Kutta method for many time steps until the sum of the time steps is equal to Δt. As before, the two steps are alternated in time through a Strang-type splitting.

IV. A MODEL PROBLEM

To examine the equations for slender vortex motion, we apply them to a well-understood model problem. Our problem comes from the theory of superfluid vortices,[24] chosen because of the wealth of analytical results available.

Superfluid helium at absolute zero temperature is inviscid and irrotational. The circulation around a vortex core is quantized and the core radius of superfluid vortices is very small (O(1 Å)). Vortex waves are a very important phenomenon in the understanding of quantized vortex lines. Wave excitations of isolated vortex lines in superfluid are considered to be helical disturbances which rotate about the axis of symmetry with a known frequency. When two helical waves are excited on a vortex line between fixed boundaries, two waves of opposite polarization combine to form a plane standing wave called a Kelvin wave.

Benjamin and Feir[25] showed that finite-amplitude waves on deep water are unstable to perturbations in the sideband waves (i.e., modes whose number of half waves are $n\pm k$, where $k=1,2,\ldots$ and n is the number of half waves for the main harmonic). The Benjamin–Feir instabilities are widespread and play an important role in nonlinear wave phenomena. In particular, Yuen and Ferguson[26] have shown that the Benjamin–Feir instabilities appear in the wave solutions

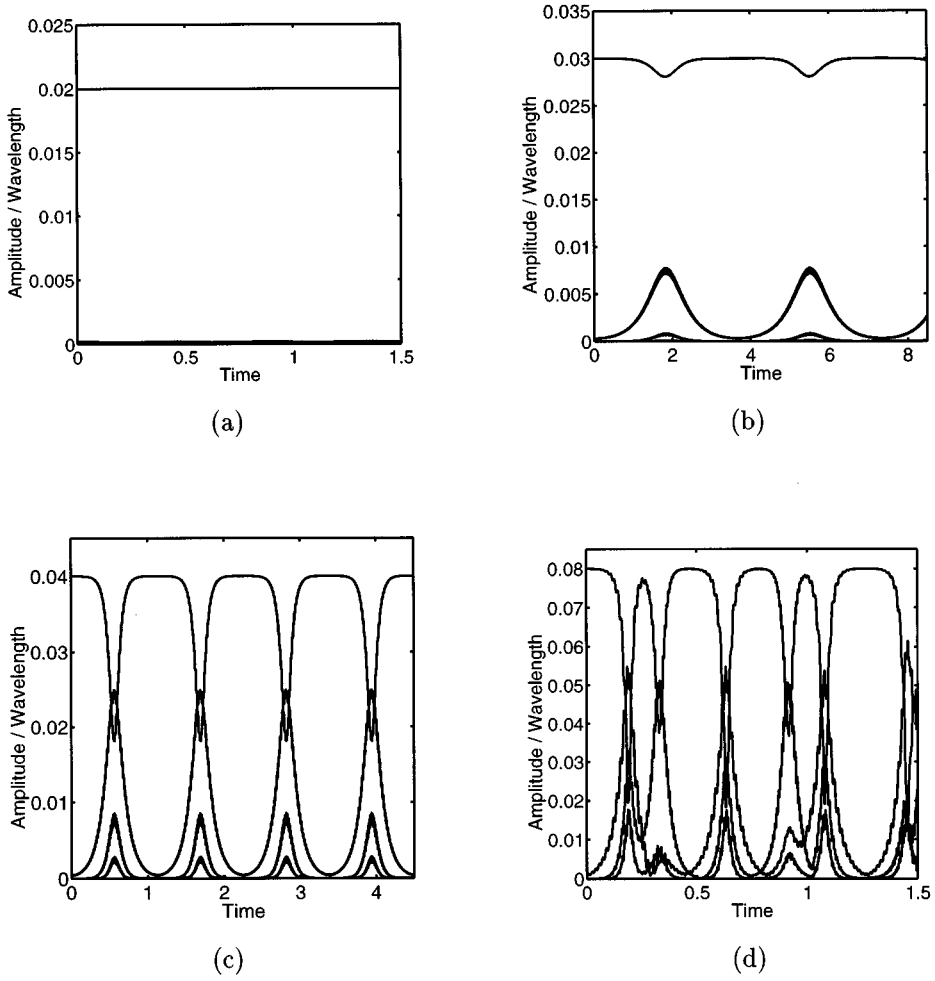

FIG. 3. Sideband instability for Kelvin waves by LIA.

to the NLSE. Since helical waves in our problem are wave solutions to the NLSE, it is not surprising that the Benjamin–Feir instabilities occur for Kelvin waves. Following the stability analysis of Andersen, Datta, and Gunshor,[27] Samuel and Donnelly[24] found that the stability condition for helical waves which obeys the NLSE is

$$a_0/\lambda < 1/(2\pi n), \tag{43}$$

where a_0 is the initial amplitude of the main helical wave, λ is the wavelength, and n is the number of half waves on the vortex. The stability condition (43) can also be obtained by a linear stability analysis following Klein and Majda.[16]

The amplitudes of the unstable sidebands grow exponentially when a_0/λ violates the stability condition (43). Once the amplitudes of the sidebands grow to be comparable in magnitude to the amplitude of the main wave, this instability analysis is invalid and a new behavior occurs. More specifically, when the initial amplitude a_0/λ is smaller than the threshold value given by (43), the amplitudes of the main harmonic and the sidebands remain unchanged. In this case, we have *stable* phenomena. If the initial a_0/λ is slightly above the threshold given by (43), the amplitudes of the sidebands grow due to Benjamin–Feir instabilities. In the meantime, the amplitude of the main carrier decreases. After some time the sidebands reach their peak amplitudes and the main carrier reaches its minimum. Then the sidebands and the main carrier return to their original amplitudes. The main harmonic and the sidebands grow and decay alternately, and the process repeats itself although not with perfect periodicity. This kind of phenomenon is normally referred to as the *Fermi–Pasta–Ulam recurrence*,[28] as opposed to Poincaré recurrence, which requires the return of both amplitude and phase to their initial states. A further increase in the initial value a_0/λ leads to a behavior which is neither stable nor recurrent. It is called *chaotic*. Those behaviors will be illustrated numerically in the following section.

V. NUMERICAL SIMULATIONS

We choose the same problem as in Samuels and Donnelly.[24] The initial condition is chosen as a vortex line between two parallel planes which are 10^{-5} m apart from each other. The initial position of the vortex line is a planar wave perturbed by two neighboring sidebands of small amplitude. In our numerical simulations, we normalize the parameters by taking the distance between the walls as a unit. Thus the dimensionless core radius of the superfluid vortex filament is $=10^{-10}/10^{-5}=10^{-5}$. The boundary conditions

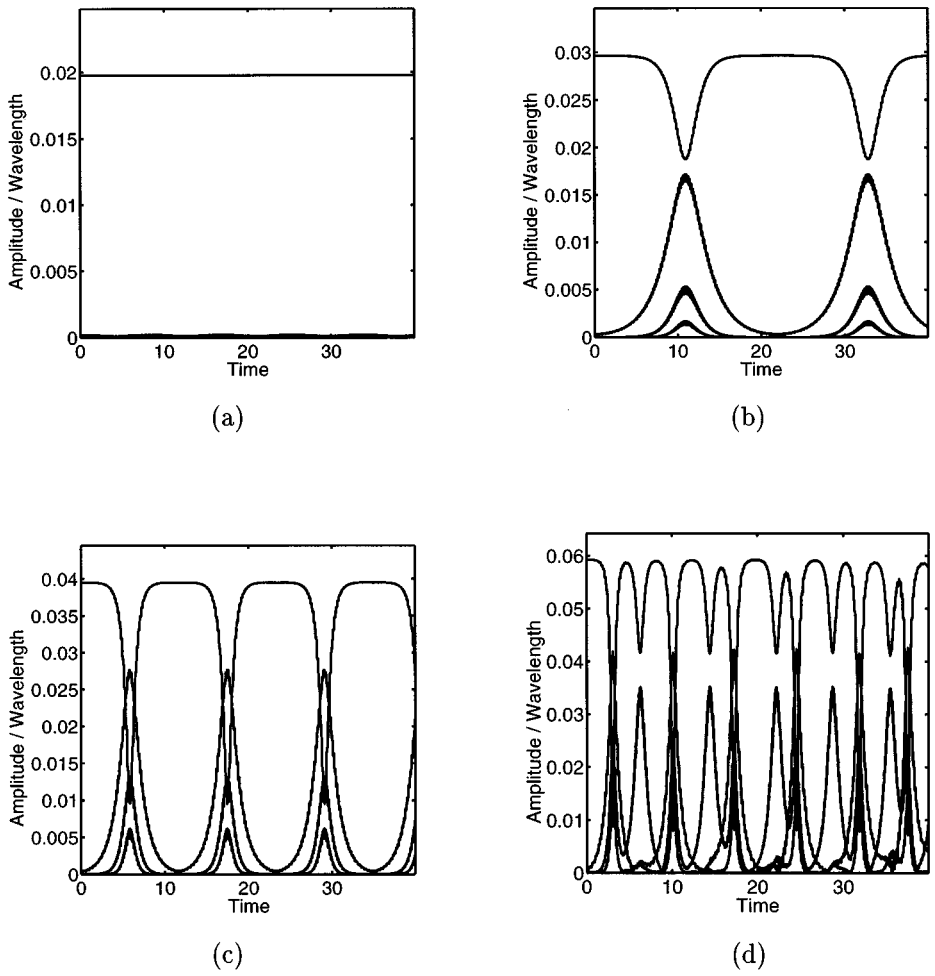

FIG. 4. Sideband instability for Kelvin waves by the Klein–Majda model.

are that the vortex line must meet the boundaries perpendicularly and can slip along the boundaries. These conditions can be implemented by the method of images. One reflects the filament once with respect to one of the boundaries and then extends it periodically. In our numerical simulations, as we advance the vortex filament in time, we decompose the filament curve into Fourier modes. In this way, we obtain the amplitudes of the main mode and its sidebands as functions of time t.

In Fig. 3 we present the results given by the self-induction equation. The x-axis is the time, whereas the y-axis is the ratio of the amplitude to the wavelength λ. Plotted in Fig. 3 are the amplitude of the main harmonic ($n=11$) and the lower harmonics ($n=10$, 9, 8 in order of decreasing amplitude) as a function of time. The plot of the upper harmonics ($n=12$, 13, 14) looks very similar. When the ratio of the initial amplitude of the main harmonic a_0 to its wavelength λ is 0.02, the amplitudes of the sideband waves do not grow [Fig. 3(a)] and we obtain stable phenomenon. If the initial a_0/λ is increased to 0.03 [Fig. 3(b)] or 0.04 [Fig. 3(c)], a recurrent behavior is observed. When a_0/λ is further increased to 0.08 [Fig. 3(d)], a chaotic behavior occurs. These results confirm the stability condition (43). During the evolution of the filament, the total arclength is conserved. In the calculations which lead to Fig. 3, we used $N=257$ nodes to represent the vortex filament between the walls; a midpoint rule was used to recover the position vectors from the tangent vectors.

The numerical results given by the Klein–Majda model for $a_0/\lambda=0.02$, 0.03, 0.04, and 0.06 are shown in Figs. 4(a), (b), (c), and (d). Similar to what we see in Fig. 3, stable, recurrent, and chaotic behaviors are also observed here. Figure 4 was obtained with $N=257$ and $\varepsilon=0.309$ which is related to the core size through the distinguished limit (11).

Figures 5(a), (b), (c), and (d) display the results by the Klein–Knio model corresponding to initial values of $a_0/\lambda=0.03$, 0.04, 0.06, and 0.08. Again, stable, recurrent, and chaotic behaviors are exhibited. The evolution of the vortex filament by the Klein–Knio equation keeps the total arclength almost a constant. The results in Fig. 5 were obtained with $N=513$ and $\delta^{\mathrm{ttm}}=0.01$.

We want to point out that even though our graphs representing the ''chaotic'' cases are shown only for a few oscillations, our calculations show that as time increases, they become more and more chaotic and they do not exhibit any recurrency.

The above numerical experiments indicate that the self-induction equation, the Klein–Majda model, and the Klein–Knio model yield qualitatively similar results for our model problem. However, they do have some quantitative differ-

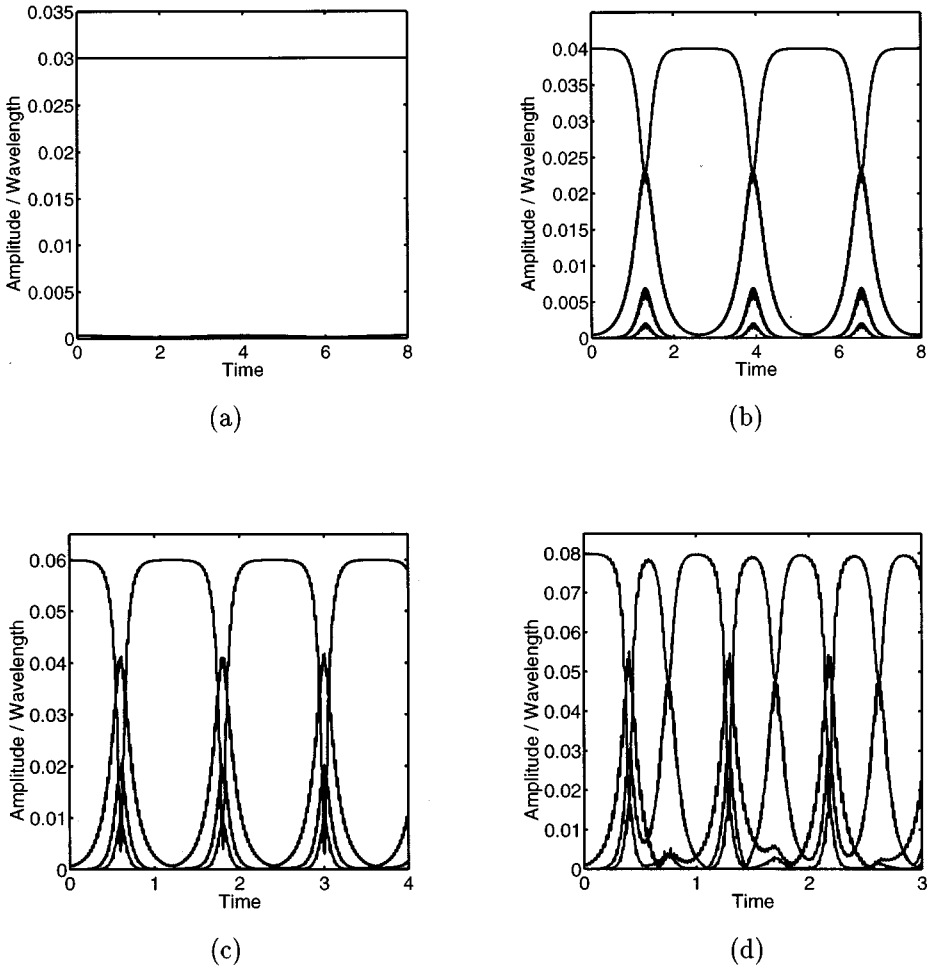

FIG. 5. Sideband instability for Kelvin waves by the Klein–Knio model.

ences. The boundaries between stable, recurrent, and chaotic regimes in the parameter space (i.e., initial values of a_0/λ) are different for these models. A comparison of Fig. 5(a) and Fig. 3(b) shows that the Klein–Knio equation has a larger stability region than that of the self-induction equation, since for the same initial value $a_0/\lambda = 0.03$, the self-induction equation gives unstable (recurrent) behavior, whereas the Klein–Knio model gives stable behavior. Further numerical experiments reveal that the stability region of the Klein–Knio model is related to the core size: A larger core size generates a larger stability region.

To compare the self-induction equation and the Klein–Majda model, we plot the stability diagram for both the Klein–Majda model and the NLSE in Fig. 6 for $\varepsilon = 0.5$ [Fig. 6(a)], $\varepsilon = 0.4778$ [Fig. 6 (b)], $\varepsilon = 0.309$ [Fig. 6 (c)], and $\varepsilon = 0.1$ [Fig. 6 (d)]. The solid lines are for the Klein–Majda model and the dashed lines are for the NLSE. The horizontal axis is a_0/λ, and the vertical axis is the growth rate G. Instability occurs for negative G. As shown in Fig. 6, the stability behavior of the Klein–Majda model depends on the parameter ε. More precisely, if $\varepsilon > 0.4778$, the Klein–Majda model always gives stable behavior. When $\varepsilon < 0.4778$, the Klein–Majda model has a smaller stable region than that of the NLSE. As ε is further decreased, the stability region of the Klein–Majda model eventually converges to that of the NLSE. For our model problem, the parameter ε is approximately 0.309, hence the self-induction equation has a larger stability region than that of the Klein–Majda model.

All of the above simulations have assumed a quasi-steady core structure for the thin vortex filament. Now we want to examine what happens if the core structure is not quasi-steady and the initial discrete core structure may not satisfy the quasi-steadiness requirement. For this purpose, we use standard vortex method to simulate the behavior of the vortex filament. The standard vortex method uses a finite collection of vortex filaments with overlapping cores to approximate the vorticity field. It makes no assumption on the physical vorticity. For the theoretical, numerical, computational, and physical aspects of vortex methods, one can see, for example, Beale and Majda,[29,30] Chorin,[10] Leonard,[31] and Puckett.[32] In our computation, we used 7 vortex filaments to approximate the cross-section of the physical vortex filament. Each of these 7 numerical filaments initially has the same shape of Kelvin waves and is represented by 200 vortex elements. The calculation is terminated if there is a filament with more than 1000 elements. A fourth-order Runge–Kutta method was used to advance the filaments with time step Δt controlled by $\Delta t \cdot \max|\mathbf{u}_i^n| \leqslant Ch$, where $\mathbf{u}_i^n$ is the velocity at the ith node, C is a constant and h is the spatial step

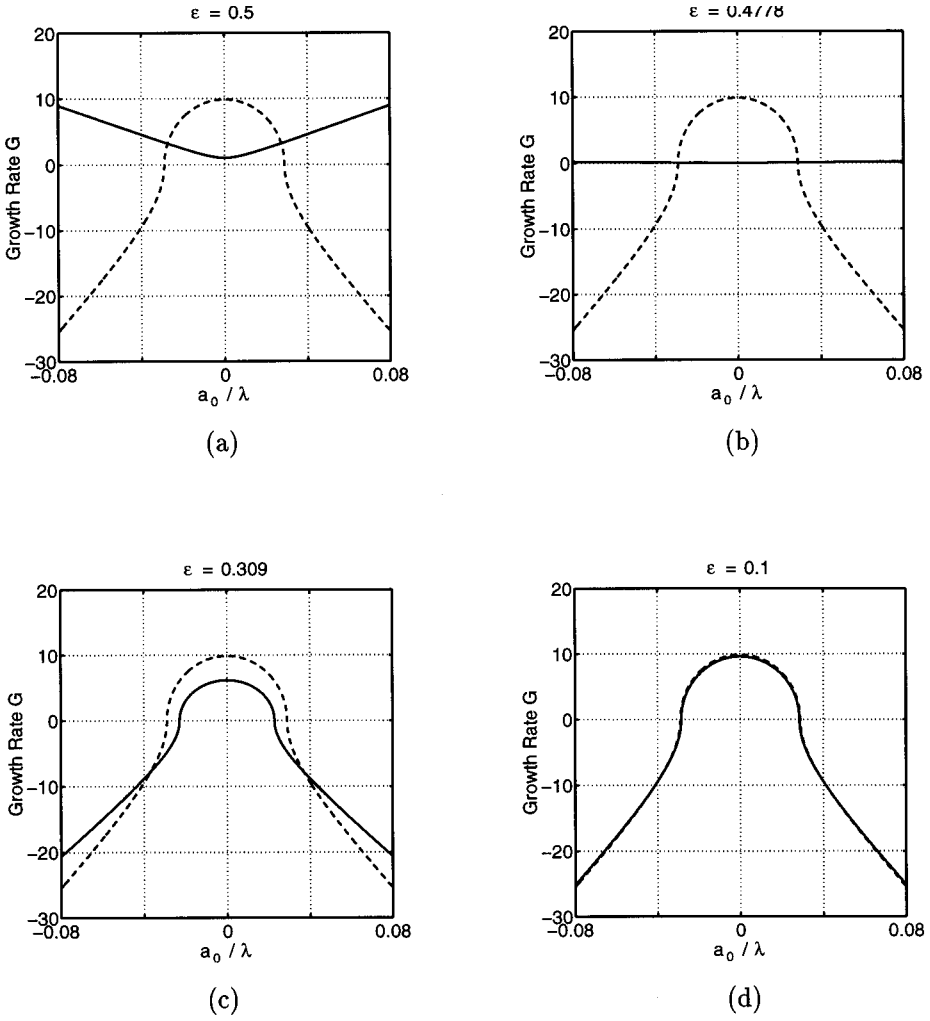

FIG. 6. Stability diagram for the Klein–Majda model and NLSE.

size. Figures 7(a) and (b) are three-dimensional perspective views of the vortex at time $t=0.4216$ and 1.9189. Here the initial value a_0/λ is taken as 0.04. Figures 7(a) and (b) show that violent stretching happens very quickly. Figures 7(c) and (d) are two-dimensional views of Figs. 7(a) and (b), respectively. It appears that the cross-section is no longer unchanged. We plot the evolution of the modes $n=8$, 9, 10 and 11 in Fig. 8 with different initial data $a_0/\lambda=0.02$, 0.04, 0.06, 0.08. The solid curve denotes the amplitude of mode $n=11$, dashed curve $n=10$, dash-dotted curve $n=9$, and dotted curve $n=8$. These results show that a vortex filament with nonquasi-steady core structure exhibits a wild behavior, which is quite different from a thin vortex filament with quasi-steady core structure. This may explain the different behavior between thick classical vortices and superfluid vortices, since superfluid vortices are postulated to have a constant core structure. For thin classical vortices, the assumption of the quasi-steady core structure is self-consistent in the asymptotic analysis.[3] However, to determine numerically whether or not a quasi-steady core structure will always remain quasi-steady requires an accurate resolution of the core structure. Currently, even with fast vortex method, we are still unable to achieve such a high resolution in the spatial discretization to settle this issue.

In all of our numerical calculations, we have carefully checked that our choices of numerical parameters provide an adequate resolution and that further refinement does not change the conclusions. More specifically, numerical solutions of the three models for slender vortex filament have converged in the sense of maximum norm. The convergence of a numerical solution by standard vortex method is a subtle issue. For the standard vortex method, the traditional pointwise convergence is not expected. Here the conclusion we draw from the numerical solutions of standard vortex method is that a thick vortex filament (i.e., wavelength of the perturbation wave is not small compared to the core size) does not maintain a quasi-steady core structure. This conclusion is not changed when the numerical mesh is refined. Also this conclusion is supported by the calculations of Chorin.[34] The oscillations in Figs. 3, 4 and 5 are probably due to the effect of other sidebands and the effect of the nonlinear Hasimoto transformation from the filament function to filament curve. In the stability analysis, we keep only three modes $n-1$, n, and $n+1$. Thus the effects of other sidebands (for ex-

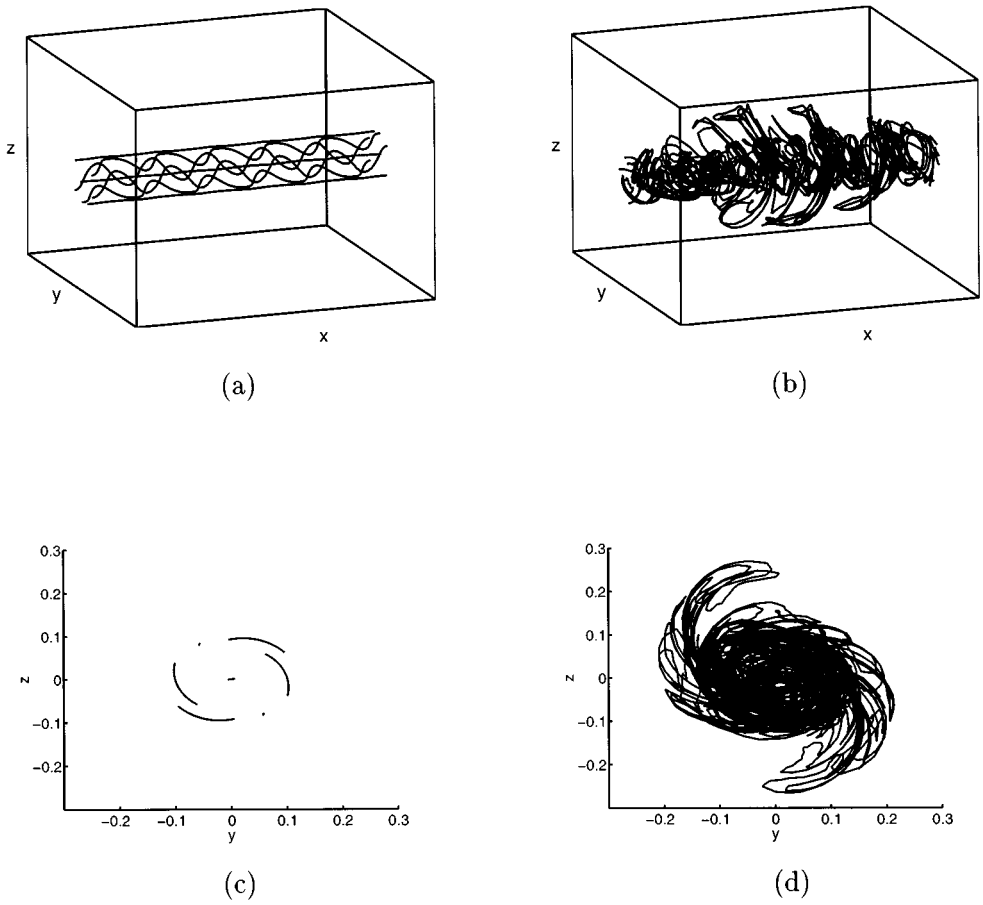

FIG. 7. Perspective views of the vortex.

ample, $n-2$, $n+2$, etc.) are ignored. Also in the stability analysis, we deal with the filament function instead of the filament curve. We have shown[33] that a small sideband perturbation to the filament function is, to the leading order, equivalent to a small sideband perturbation to the filament curve. Thus the small oscillation in the graphs, caused by other sidebands and the nonlinear Hasimoto transformation, does not contradict with the stability analysis.

VI. CONCLUSIONS

We have used three different equations, namely the self-induction equation, the Klein–Majda equation, and the Klein–Knio equation, to study the sideband instability of Kelvin waves in superfluid helium. In this model problem, we assume that the thin vortex filament has constant cross-section.

Our numerical simulations reveal that all those methods yield qualitatively similar results. For our model problem, the self-induction equation, the Klein–Majda equation, and the Klein–Knio equation all present stable, recurrent, and chaotic phenomena, corresponding to different ratios of the amplitude of the main wave to its wavelength. The vortex filament whose motion is described by the self-induction equation, the Klein–Majda equation or the Klein–Knio equation evolves smoothly and the total arc length is almost conserved. Furthermore, hairpin structures are not formed during the vortex filament evolution. Our calculations using the self-induction equation and the Klein–Majda equation are in good agreement with the results of the linear stability theory.

The stability region of the Klein–Majda equation is closely related to the core size of the vortex filament. When the core size is larger than a critical value, the Klein–Majda equation always gives a stable solution. When the core size is below the critical value, the stability region of the Klein–Majda equation is smaller than that of the self-induction equation. When the core size is further decreased, the stability region of the Klein–Majda equation coincides with the stability region of the self-induction equation. For the model problem, the stability region of the Klein–Majda equation is smaller than that of the self-induction equation.

The stability region of the Klein–Knio equation also depends on the core size of the vortex filament. The bigger the core size, the larger is the stability region. We further find that for the model problem, the Klein–Knio equation has a larger stability region than that of the self-induction equation. Hence, among our three equations for the model problem, the Klein–Knio equation gives the largest stability region, while the Klein–Majda equation has the smallest stability region.

We also carried out the computations for a vortex with non-quasisteady core structure. A Biot–Savart model was employed. Only chaotic phenomena were observed for sideband perturbations. Our numerical results imply that vortices

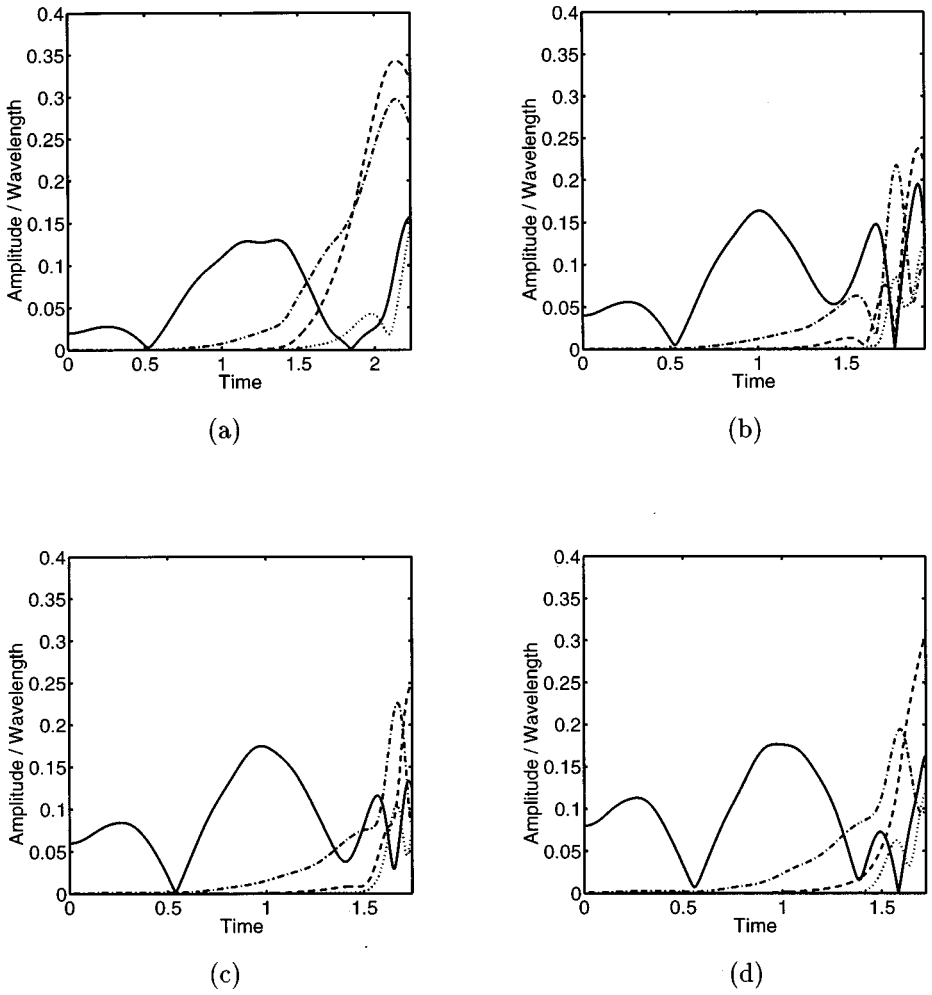

FIG. 8. Behaviors by the vortex method.

with nonquasi-steady core structure behave quite differently from thin vortices with quasi-steady core structure. The thickness and deformation of the vortex core might play an important role in the differences between classical and superfluid vortex dynamics, which have been highlighted by Buttke.[14]

In the derivations of the self-induction equation, the Klein–Majda equation, and the Klein–Knio equation, we have assumed a thin filament model, in which hairpins[34] are excluded; our numerical results have no hairpins, and therefore the thin filament model is self-consistent, at least for a class of problems that contains our model problem. Since the models are increasingly refined (i.e., the Klein–Knio model takes more effects into account than the Klein–Majda model, which in turn is a more accurate approximation than the self-induction equation), it is reasonable to conjecture that motion without hairpins is self-consistent for a class of thin vortex filaments of small-enough cross-sections.

If one views superfluid vortices as classical vortices with very thin constant cross-section, the conclusion is consistent with the statistical theory of vortex motion[7] which shows that classical vortices, with finite and deformable cross-section, have a temperature determined by vortex stretching, while superfluid vortex systems have a constant temperature determined by boundary conditions.

The difference between classical and quantum vortices are often explained as a consequence of quantization; according to our results, maybe slenderness is even more important. Of course, only very slender vortices can have a quantized circulation.

If the self-induction equation, the Klein–Majda equation, and the Klein-Knio equation are used to describe superfluid turbulence,[14,35,36] then the physical assumption that there is no vortex folding on small scale has been implicitly made. Our numerical simulations suggest that this may be a reasonable conclusion for a single filament, but is for the moment an additional assumption for a tangle of filaments. Deeper understanding remains to be found.

ACKNOWLEDGMENTS

This work is based in part on the author's Ph.D. dissertation, carried out under the supervision of Professor Alexandre Chorin. It was supported in part by the Applied Mathematical Sciences Subprogram of the Office of Energy Research, U.S. Department of Energy under Contract No. DE-AC03-76SF00098. All computations were performed at the Lawrence Berkeley National Laboratory. The author is very grateful to the referees for suggestions on improving the original manuscript.

[1]G. K. Batchelor, *An Introduction to Fluid Mechanics* (Cambridge University Press, Cambridge, 1967).
[2]R. Klein and A. Majda, ''Self-stretching of a perturbed vortex filament (I),'' Physica D **49**, 323 (1991).
[3]R. Klein and O. M. Knio, ''Asymptotic vorticity structure and numerical simulation of slender vortex filaments,'' J. Fluid Mech. **284**, 275 (1995).
[4]A. J. Chorin and J. Akao, ''Vortex equilibria in turbulence theory and quantum analogues,'' Physica D **51**, 403 (1991).
[5]A. Majda, ''Vorticity, turbulence, and acoustics in fluid flow,'' SIAM Rev. **33**, 349 (1991).
[6]A. J. Chorin, ''Turbulence and vortex stretching on a lattice,'' Commun. Pure Appl. Math. **XXXIX**, S47 (1986).
[7]A. J. Chorin, *Vorticity and Turbulence* (Springer, Berlin, 1993).
[8]A. J. Chorin, ''Vortex phase transitions in 2.5 dimensions,'' J. Stat. Phys. **76**, 835 (1994).
[9]A. J. Chorin and O. Hald, ''Vortex renormalization in three space dimensions,'' Phys. Rev. B **51**, 11 969 (1995).
[10]A. J. Chorin, '' Vortex methods,'' Les Houches Summer School of Theoret. Phys. **59** (1995).
[11]A. Almgren, T. Buttke, and P. Collela, ''A fast adaptive vortex method in three dimensions,'' J. Comput. Phys. **113**, 177 (1994).
[12]S. E. Widnall, D. B. Bliss, and C. Y. Tsai, ''The instability of short waves on a vortex ring,'' J. Fluid Mech. **66**, 35 (1974).
[13]H. Y. Wang, ''A study of short wave instability on vortex filaments,'' Ph.D thesis, University of California, Berkeley, 1996.
[14]T. F. Buttke, ''Numerical study of superfluid turbulence in the self-induction approximation,'' J. Comput. Phys. **76**, 301 (1988).
[15]H. Hasimoto, ''A soliton on a vortex filament,'' J. Fluid Mech. **51**, 477 (1972).
[16]R. Klein and A. Majda, ''Self-stretching of perturbed vortex filaments (II): Structure of solutions,'' Physica D **53**, 267 (1991).
[17]O. M. Knio and A. F. Ghoniem, ''Numerical study of a three-dimensional vortex method,'' J. Comput. Phys. **86**, 75 (1990).
[18]R. Klein, O. M. Knio, and L. Ting, ''Representation of core dynamics in slender vortex filament simulations,'' Phys. Fluids **8**, 2415 (1996).
[19]A. Callegari and L. Ting, ''Motion of a curved vortex filament with decaying core and axial velocity,'' SIAM J. Appl. Math. **15**, 148 (1978).
[20]J. T. Beale and A. Majda, ''High order accurate vortex methods with explicit velocity kernals,'' J. Comput. Phys. **58**, 188 (1985).
[21]T. F. Buttke, ''A numerical study of superfluid turbulence in the self-induction approximation,'' Ph.D thesis, University of California, Berkeley, 1986.
[22]P. J. Prince and J. R. Dormand, ''High order embedded Runge–Kutta formulae,'' J. Comput. Appl. Math. **7**, 67 (1981).
[23]D. Laugwitz, *Differential and Riemannian Geometry* (Academic, New York, 1960).
[24]D. C. Samuels and R. J. Donnelly, ''Sideband instability and recurrence of Kelvin waves on vortex core,'' Phys. Rev. Lett. **64**, 1385 (1990).
[25]T. B. Benjamin and J. E. Feir, ''The disintegration of wave trains on deep water,'' J. Fluid Mech. **27**, 417 (1967).
[26]H. C. Yuen and W. E. Ferguson, Jr., ''Relationship between Benjamin–Feir instability and recurrence in the nonlinear Schrödinger equation,'' Phys. Fluids **21**, 1275 (1978).
[27]D. R. Andersen, S. Datta, and R. J. Gunshor, ''A coupled mode approach to modulation instability and envelope solitons,'' J. Appl. Phys. **54**, 5608 (1983).
[28]E. Fermi, S. Ulam, and J. Pasta, ''Studies on non linear problems,'' in *Collected papers of Enrico Fermi II*, edited by E. Segré (University of Chicago, Chicago, 1965).
[29]J. Beale and A. Majda, ''Vortex method I: Convergence in three dimensions,'' Math. Comput. **39**, 1 (1982).
[30]J. Beale and A. Majda, ''Vortex method II: High order accuracy in two and three dimensions,'' Math. Comput. **39**, 29 (1982).
[31]A. Leonard, ''Computing three-dimensional incompressible flows with vortex elements,'' Annu. Rev. Fluid Mech. **17**, 523 (1985).
[32]E. Puckett, ''Vortex methods: An introduction and survey of selected research topcis,'' in *Incompressible Computational Fluid Dynamics Trends and Advances* (Cambridge, 1993).
[33]H. Zhou, ''Numerical analysis of slender vortex motion,'' Ph.D thesis, University of California, Berkeley, 1996.
[34]A. J. Chorin, ''Hairpin removal in vortex interactions,'' J. Comput. Phys. **91**, 1 (1990).
[35]R. J. Donnelly, ''Quantized vortices in helium II,'' Annu. Rev. Fluid Mech. **25**, 325 (1993).
[36]K. W. Schwarz, ''Generation of superfluid turbulence deduced from simple dynamical rules,'' Phys. Rev. Lett. **49**, 283 (1982).